frontiers | Frontiers in Earth Science

TYPE Original Research
PUBLISHED 20 September 2022
DOI 10.3389/feart.2022.1016122

OPEN ACCESS

EDITED BY
Yuqi Wu,
China University of Petroleum, China

REVIEWED BY
Zhipeng Huo,
Northeastern University at Qinhuangdao, China
Hongjian Zhu,
Yanshan University, China
Jianglin He,
China Geological Survey, China
Cui Mao,
Northeast Petroleum University, China

*CORRESPONDENCE
Zhe Liu,
liuzhe@gdupt.edu.cn

SPECIALTY SECTION
This article was submitted to Solid Earth Geophysics, a section of the journal Frontiers in Earth Science

RECEIVED 10 August 2022
ACCEPTED 07 September 2022
PUBLISHED 20 September 2022

CITATION
Li J, Fu G, Zhu D, Cao L, Li Z, Lv Y, Li W, Hu M and Liu Z (2022), Reservoir characteristics and factors influencing shahejie marl in the shulu sag, bohai bay basin, eastern China.
Front. Earth Sci. 10:1016122.
doi: 10.3389/feart.2022.1016122

Reservoir characteristics and factors influencing shahejie marl in the shulu sag, bohai bay basin, eastern China

Jiajing Li[1,2], Guang Fu[1], Douxing Zhu[3], Lanzhu Cao[4], Zhaolong Li[5], Yanfang Lv[1], Wenke Li[6], Ming Hu[2] and Zhe Liu[2]*

[1]School of Earth Sciences, Northeast Petroleum University, Daqing, Heilongjiang, China, [2]School of Petroleum Engineering, Guangdong University of Petrochemical Technology, Maoming, Guangdong, China, [3]Geological Research Center, GRI, BGP Inc., CNPC, Zhuozhou, Hebei, China, [4]PetroChina Huabei Company, Renqiu, Hebei, China, [5]No.1 Data Acquisition Branch Company, No.1 Geo-Logging Company, Daqing Drilling and Exploration Engineering Corporation, Daqing, Heilongjiang, China, [6]The Research Institute of Petroleum Exploration and Development, Beijing, China

Shahejie marl in the Shulu Sag is a crucial resource for unconventional hydrocarbon exploration in China. Although breakthroughs have been made in tight oil exploration in this area, the mechanisms underlying the formation of this marl reservoir and factors controlling its 'sweet spots' have not been thoroughly studied. To understand the pore structure characteristics and factors influencing the marl reservoir, we analyzed core samples from Wells ST1 and ST3. A series of experiments was conducted on the samples, such as X-ray diffraction, focused ion beam scanning electron microscopy, micro-CT, and total organic carbon test. Additionally, the physical properties of different marl rock fabrics were studied with auxiliary tests, such as mercury intrusion capillary pressure analyses, nuclear magnetic resonance, porosity and permeability tests, and thin-section observation. The results revealed that the marl reservoir is characterized by low porosity (1.61%) and low permeability (2.56mD). The porosity and permeability (1.61% and 3.26mD) of laminated marl were better than those (0.92% and 1.68mD) of massive marl. Clay minerals and quartz content in laminated (11.8 and 8.2%) was less than in massive marl (16.2 and 13.3%). The marl pores include intercrystalline pores, dissolution pores, and microfractures. Additionally, the laminated marl pores were primarily distributed along the dark lamina, with good connectivity. A few isolated and uniform holes were observed in the massive marl. Influenced by rock fabric and mineral composition, layered fractures were mainly developed in the laminated marl, while structural fractures were the main type of microfractures in the massive marl. The primary sedimentary mechanism was the main geological action underlying the differences in marl rock fabric; this mechanism affects the physical properties of the marl reservoir, which are key factors to be considered when searching for the marl reservoir 'sweet spots'. Particular attention should be paid to these factors during tight oil exploration and development in similar sedimentary basins.

KEYWORDS

marl, tight reservoir, pore structure, reservoir characteristics, tight oil, shulu sag

Introduction

Tight oil, an important unconventional hydrocarbon energy resource, has attracted considerable attention from major oil companies worldwide (Jia et al., 2012a; Jia et al., 2012b; Zou et al., 2012). Since the discovery of tight hydrocarbon energy in Bakken, Eagle Beach, and other areas in the USA and North America, tight oil has emerged as an important hot spot in the oil exploration industry (He et al., 2018; James et al., 1983; Jiang and Mokhtari, 2019; Lin et al., 2011; Miller et al., 2008). Tight oil reservoirs are often characterized by low porosity and ultra-low permeability, severely restricting the pace of tight oil as well as gas exploration and development (Jia et al., 2012a; Shan et al., 2017; Hou et al., 2018; Li et al., 2022). Therefore, finding a reservoir 'sweet spot' suitable for oil and gas production is quintessential.

China has made considerable progress in the exploration of tight hydrocarbon reservoirs. A set of marlstones formed by lacustrine carbonate lime-mud and terrigenous carbonate clasts are present in the Shulu Sag, Bohai Bay Basin (Qiu et al., 2010; Zhao et al., 2015; Cui et al., 2021). The marl has a high organic matter content, large thickness, and wide dispersion. This marl is the main source of hydrocarbons, even though it is the main tight hydrocarbons reservoir (Zhao et al., 2014a). The ST1 and ST3 wells drilled in the study area yielded industrial oil flow, offering good tight oil exploration prospects (Zhao et al., 2014b). With the breakthrough of hydrocarbon exploration in the Shulu Sag marl, several notable achievements have been made in studying reservoir characteristics. For instance, a multi-dimensional lithologic classification scheme for marl was established based on rock fabric and mineral composition (Cui et al., 2015). The marl can be divided into structural, interbedded, and mixed rock and is characterized by nine lithofacies (Jiang et al., 2007; Liang et al., 2007). Furthermore, with respect to its genesis, marl can be categorized as seasonal and turbidite (Kong et al., 2020, 2016). Due to technical limitations, the reservoir spaces, reservoir properties, and factors underlying the marl-based reservoir are still unclear (Han et al., 2015; Liu et al., 2020; Liu et al., 2022a); thus, the exploration of tight hydrocarbons in the Shulu Sag remains in the preliminary stage.

Reservoir research is one of the most important steps in the exploration and development of unconventional hydrocarbon resources. However, traditional experimental methods can no longer meet the needs of tight oil and gas reservoirs in terms of microscopic pore structure, physical properties, and diagenetic mineral content. Moreover, the measurement accuracy, efficiency, and visualization of measurement results can hardly meet the needs of the industry. With the rapid development of scanning electron microscopy (SEM), graphics processing technologies, and machine learning, digital rock physics has become an important and effective means to analyze of reservoir pore microstructure and predict effective physical properties of porous media in the petroleum industry (Zhao et al., 2016; Liu and Grana, 2018; Wu et al., 2018, 2019a, 2020a, 2022a; Bordignon et al., 2019; Qian et al., 2022). The marl of the Shahejie Formation is a key horizon for tight oil exploration in the Shulu Sag; however, the processes underlying the reservoir formation, microscopic pore structure, and factors controlling the reservoir 'sweet spots' have not been rigorously studied. Here, we obtained samples from wells ST1 and ST3. SEM was used to analyze the 2D pore structure of the samples, whereas the 3D pore structure was revealed by a field emission scanning electron microscope (FE-SEM) and micro-CT measurements. Concomitantly, combined with other testing methods, such as mercury intrusion capillary pressure (MICP) analyses, total organic carbon (TOC) content analyses, X-ray diffraction (XRD), porosity and permeability tests, and thin-section observations, the oil storage capacity of marl samples differentiated along the lines of rock fabric were studied, which is essential for understanding the accumulation of tight oil in the Shulu Sag.

Geological setting

The Shulu Sag is located south of the Jizhong Depression of the Bohai Bay Basin in eastern China (Figure 1A) (Zhou et al., 2020). It is a long, narrow dustpan fault depression formed in the Paleozoic crystalline basement. The Shulu Sag is bounded by the Xinhe Fault in the east, Ningjin Uplift in the west, and the Shenxian Sag in the north through Hengshui Fault, covering an area of ~ 700 km^2 (Figure 1B; Fu et al., 2019). The Shahejie and Dongying formations of the Paleogene, the Guantao and Minghuazhen formations of the Neogene, and the Quaternary strata are developed from bottom to top in this depression (Figure 1C, Figure 2).

The Ningjin Uplift west of the Shulu Sag is an important provenance area. Under the influence of the Ningjin Uplift, carbonate conglomerate and mixed marl exist mainly in the Es_3^x members (Zhang et al., 2021). The marl is mostly formed in a semi--to-deep lake environment (Han et al., 2015; Li et al., 2016; Huo et al., 2020). In recent years, significant breakthroughs have been made in tight oil exploration in the Shulu Sag. Specifically, 20 wells have been drilled, 17 of which encountered oil and gas, and five yielded industrial oil flow. Drilling revealed that the marl is mainly distributed in the gentle slope zone and trough area of the sag. Overall, the marl is a wedge-shaped sedimentary body with thickness ranging from 100 to 1,500 m, with the greatest thickness being in the center of the sag.

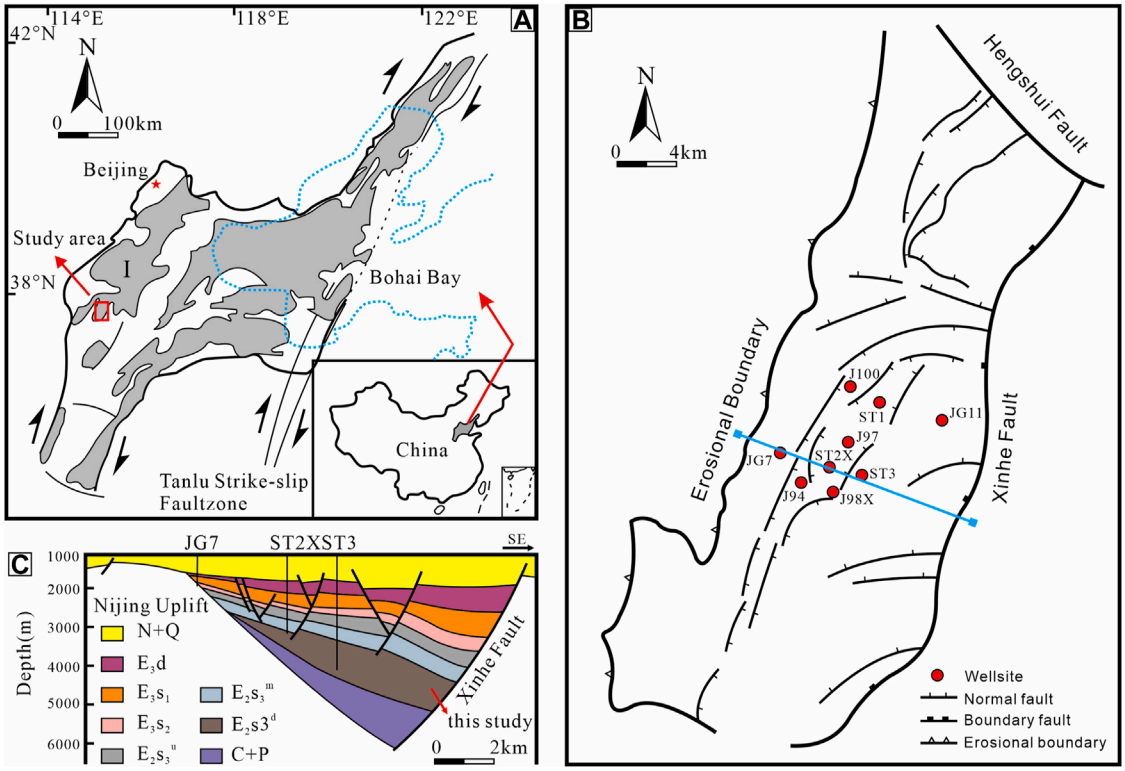

FIGURE 1
Location and structural map of the Shulu Sag: **(A)**, tectonic setting of the Shulu Sag, located in the southwestern corner of the Jizhong Depression (I); **(B)**, structural outline map of the Shulu Sag; **(C)**, transverse section across the middle segment of the Shulu Sag, the position of the section is represented as a blue line in **(B)**.

Samples and experimental methods

Sampling

More than 100 core samples were collected from wells ST1 and ST3 in the Jizhong Depression Shulu Sag (Figure 1B). All samples were chosen among the Es_3^x members. A total of 13 core samples were thoroughly studied using a variety of methodologies; specifically, these samples consisted of six and seven core samples from the laminated and massive marls, respectively. The sample information is shown in Table 1.

Experimental methods

Petrological analysis

The core samples were cut into thin pieces and examined under a polarized light microscope and a cathodoluminescence microscope, allowing the fabric of the rock to be identified.

A TTR-type XRD device was used to analyze the mineral component of core samples. Powdered samples (300 mesh size) were soaked with ethylene glycol for 8 h at 60 °C before being heated for 3 h at 550°C (Cui et al., 2021). To collect specimens, minerals were removed from the solution. Air-dried specimens were X-rayed with a diffractometer outfitted with a Cu-target Ceramic X-ray tube with emissive and receiving slits of 0.6 and 8 mm, respectively. The Rochquan+2012 program, developed by The Research Institute of Petroleum Exploration and Development (RIPED), was used to calculate the mass percentage of each mineral.

The TOC test was carried out on the samples using the LCO CS230 instrument, following the Chinese National Standard method GB/T 19145–2003 (He et al., 2018).

To identify pore types and morphologies in the samples, a Quanta 650 FE-SEM was employed. The resolution and accelerating voltage of the SEM were 1.2 nm and 30 kV (Zhang et al., 2020), respectively.

Porosity and permeability measurements

Porosity and permeability tests were outsourced at PetroChina Huabei Oilfield Company. Core plugs with a diameter of 2.5 cm and length of 5 cm were drilled from the

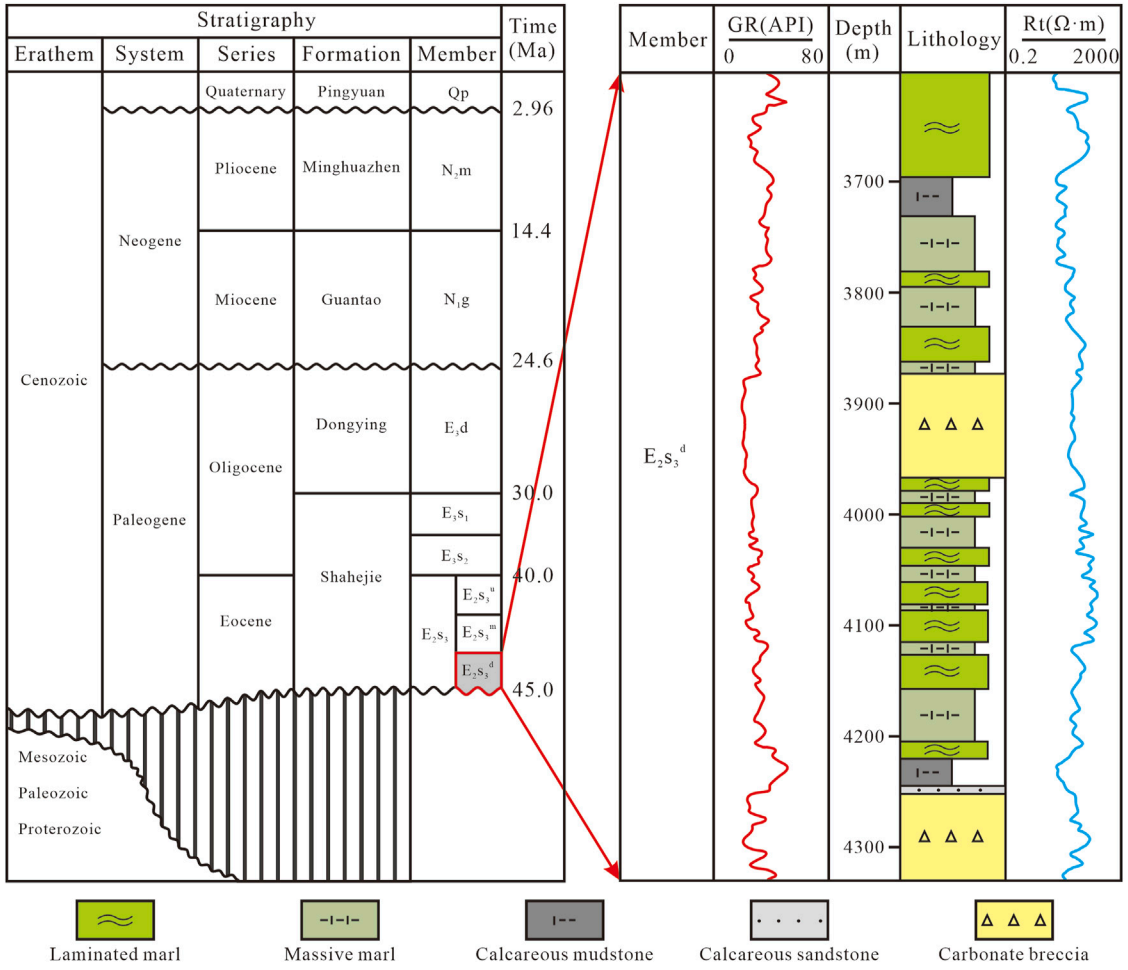

FIGURE 2
Stratigraphic systems of the Shulu Sag.

massive and laminated marl. Using Boyle's law, the porosity of core samples was measured using Ultra-pore 200A and the He permeability of core samples was measured using Ultra-perm TM200. The core plug was cleaned in benzene and alcohol for 1 month to remove residual oil, dried, and finally analyzed for petrophysical properties. The test methods were conducted per the Chinese National Standard method SY/T5336-2006 (Zhang et al., 2018).

Pore-throat structure analysis

Thirteen core plugs (25 × 25 mm) were subjected to MICP analysis with the Auto Pore IV equipment at the State Key Laboratory of China University of Petroleum (Beijing) to assess the pore architecture and pore throat distribution. A throat radius of 6 nm corresponds to a mercury intrusion pressure maximum of 200 MPa. The test premise for the experiment was SY/T5346-2005/4, and conditions were 18°C (room temperature) and 55% humidity (Zhang et al., 2020). The injection curves and other data were acquired to assess the properties of pore-throat structures.

Under 100% water saturation, the nuclear magnetic resonance (NMR) T_2 spectrum of each core sample was produced using the NUMAG's C12-010 V low-field NMR spectrometer. The three-dimensional pictures of nano- and micron-scale pores were characterized using CT scanning technology (Wu et al., 2020b, 2020c; Liu et al., 2022b; Guo et al., 2022; Liu et al., 2022), which facilitated the analysis of the marl micropores and their three-dimensional connectivity. An Ultra XRM-L200 microscope was used to perform a three-dimensional CT scan of the full-diameter core samples (XRM). The equipment included a 150 kV/15 W high-power focus X-ray tube with a maximum resolution of 1.0 μm. Cylindrical core samples were mounted vertically onto the sample holder to ensure a central field of view for the scanner. Each sample was scanned using a conical ion beam emitted from the X-ray

TABLE 1 Mineral composition, total organic carbon, and porosity of the samples from well ST1.

Sample ID	Rock type	Depth/m	Rock mineral composition (wt%)						TOC (%)	Porosity (%)
			Clay	Quartz	Calcite	Dolomite	Feldspar	Pyrite		
LM1	Laminated marl	3678.1	16.95	11.10	57.95	11.84	0.00	2.15	1.2	1.8
LM2		3789.5	9.86	5.92	70.01	12.16	1.24	0.80	1.1	0.9
LM3		3850.4	10.92	3.81	74.24	9.62	0.00	1.41	0.6	0.9
LM4		3975.3	13.99	18.82	46.32	12.59	1.23	7.05	0.2	1.1
LM5		4001.2	7.96	3.81	81.01	5.50	0.00	1.72	1.8	1.5
LM6		4048.6	7.96	8.04	66.42	16.50	0.00	1.09	1.9	1.4
LM7		4152.3	13.78	8.35	65.78	10.36	0.00	1.72	2.1	0.8
LM8		4220.5	13.04	5.92	37.86	37.02	0.00	6.17	1.5	1.1
MM1	Massive marl	3721.5	15.00	22.98	45.12	15.84	0.00	1.05	1.4	1.4
MM2		3768.3	14.81	7.18	64.81	11.21	0.00	1.99	1.5	0.7
MM3		3818.4	18.96	8.65	52.45	16.84	0.00	3.10	0.8	0.8
MM4		3875.3	34.81	13.21	37.78	8.10	2.14	3.98	1.4	0.9
MM5		3985.6	17.13	24.45	37.50	19.00	0.74	1.19	0.7	1.0
MM6		4015.7	12.88	16.82	61.24	6.98	0.95	1.14	1.2	1.7
MM7		4064.1	8.92	10.93	35.09	45.07	0.00	0.00	2.3	1.0
MM8		4089.4	5.05	9.81	34.00	49.92	0.00	1.22	2.6	1.1
MM9		4122.1	8.14	6.54	69.12	15.04	0.00	1.15	1.9	1.3
MM10		4174.6	11.81	7.16	64.98	14.06	0.00	1.99	1.4	0.6
MM11		4236.2	30.89	18.10	31.90	17.18	0.74	1.19	1.8	1.1

source. The X-ray intensity was attenuated as it passed through the sample, and these signals were recorded by the detector. Samples were rotated and scanned at different angles, yielding a 360° perspective. The NMR experiment and CT scans were conducted in RIPED.

Results

Petrographical characteristics and oil-bearing properties

In this study, the rock fabric of the marl was divided into laminated and massive marl to facilitate a structured discussion of the entire tight marl reservoir (Fu et al., 2019). The rhythmic layer consisting of alternating laminae was observed microscopically (Figure 3). The bright lamina was mainly of chemical precipitation origin, and the mineral composition mainly consisted of micritic and microcrystalline calcite and dolomite, with an orange-red cathode luminescence (Figures 3B,D,F). The dark lamina was mainly of mechanical deposition origin, and the mineral composition primarily consisted of, micritic calcite and dolomite, argillaceous, carbonate sand, quartz, organic matter, and pyrite. The cathode luminescence color was dark and scattered (Figures 3B,D,F). Laminated marl was deposited by interbedded mixing. The laminae of laminated marl were mainly in three forms: 1) Thin dark gray mudstone and light micritic limestone interbedded in unequal thickness, with parallel or non-parallel laminae boundaries (Figures 3A,B). These were formed in a still-water environment with few terrigenous materials, mainly carbonate water deposits. 2) Continental clay-bearing calcitic mudstone interbedded with micritic limestone with or without mud, and thin silt-fine sandstone interbeds that commonly occur (interbedded intercalation) with parallel lamination boundaries (Figures 3C,D). This mudstone was formed in the offshore deep-water areas or terrigenous deep-water environments with sufficient intermittent supply. 3) A grain boundary clear wavy grain layer (Figures 3E,F) formed on steep slopes, resulting in deposit layers that were not consolidated, due to slope sliding deformation dynamics. The massive marl was mainly formed through mixed structural deposition and was divided into terrigenous and endogenous components. The former component, containing argillaceous and carbonate rock of terrigenous clastic rich in organic matter (mainly consisting of calcite), was prioritized. This component also contained a bit of quartz, feldspar, and other terrigenous clastic material, occasionally interspersed with unevenly distributed granular pyrite unevenly distributed within (Figure 3G); the cathode luminescence was distorted and dark (Figure 3H). The latter component primarily contained *in situ* sedimentary micritic calcite, with only a little terrigenous carbonate arene, quartz,

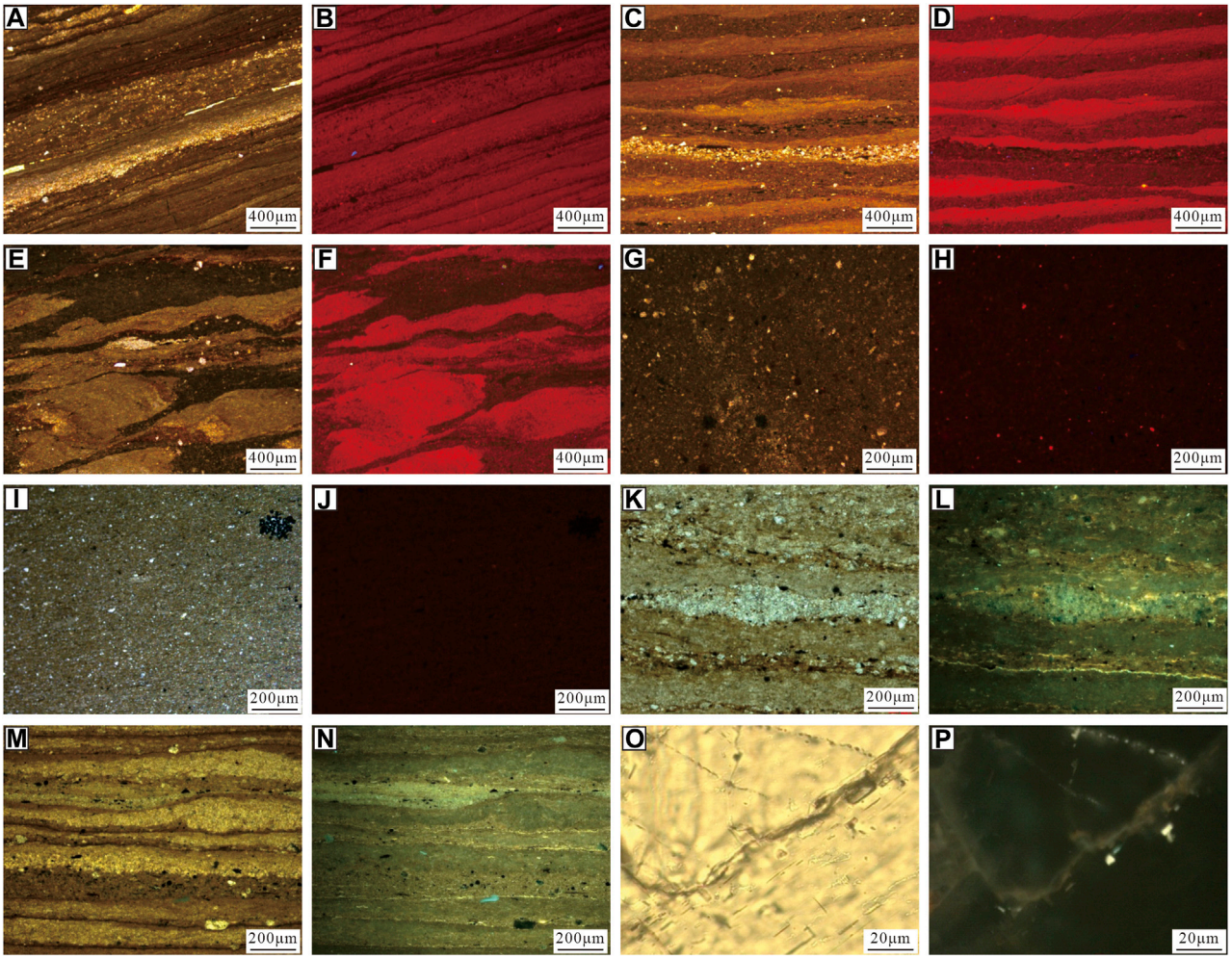

FIGURE 3
Petrographic characteristics of marl reservoir under single polarization **(A,C,E,G,I,K,M,O)**, cathode luminescence **(B,D,F,H,J)**, and fluorescence microscopy **(L,N,P)**: **(A,B)**, laminated marl with different lamina thickness, ST3, 3,664.9 m; **(C,D)**, laminated marl of equal lamina thickness, ST3, 3,681.49 m; **(E,F)**, wavy laminated marl, ST3, 3,677.61 m; **(G,H)**, terrigenous massive marl, ST3, 3,817.65 m; **(I,J)**, endogenous massive marl, ST3, 4097.06 m; **(K,L)**, laminated marl of mechanical origin, ST3, 3,978.76 m; **(M,N)**, laminated marl of chemical origin, ST3, 3,675.09 m; **(O,P)**, massive marl, ST3, 3,983.83 m.

feldspar, and clay minerals (Figure 3I); this component exhibited orange cathodoluminescence that was relatively homogenous (Figure 3J).

The thin fluorescent thin section shows that the lamina of mechanical deposition was oil-bearing in the laminated marl. Crude oil molecules were distributed along the lamina in a banded and non-uniform manner (Figure 3K, Figure 3L). The occurrence of crude oil molecules was characterized by oil in various matrix micropores, oil in lamina cracks, and adsorption of organic matter bands. The micritic limestone lamina of chemical sedimentary origin contained less oil, and crude oil molecules were evenly distributed (Figure 3M, Figure 3N). The massive marl crude oil was mainly enriched in matrix pores or structural fractures (Figure 3O, Figure 3P). In terms of oil enrichment and oil content, the oil-bearing properties of laminated marl were better than those of massive marl.

As shown in Table 1, the minerals in the marl in the Shulu Sag included calcite, dolomite, clay minerals, quartz, pyrite, and feldspar. In terms of mineral composition, laminated and massive marl mainly consisted of calcite and dolomite. The average content of calcite and dolomite in laminated marl was 62.4 and 14.4%, respectively (Figure 4A); the average content of these two minerals in massive marl was 48.5 and 19.9%, respectively (Figure 4B). The contents of clay minerals and quartz were 11.8 and 8.2%, in laminated marl and 16.2 and 13.3%, in massive marl, respectively. The average pyrite content in laminated and massive marl was 2.8 and 1.6%, respectively, while the marl of these two fabrics contained little to no feldspar.

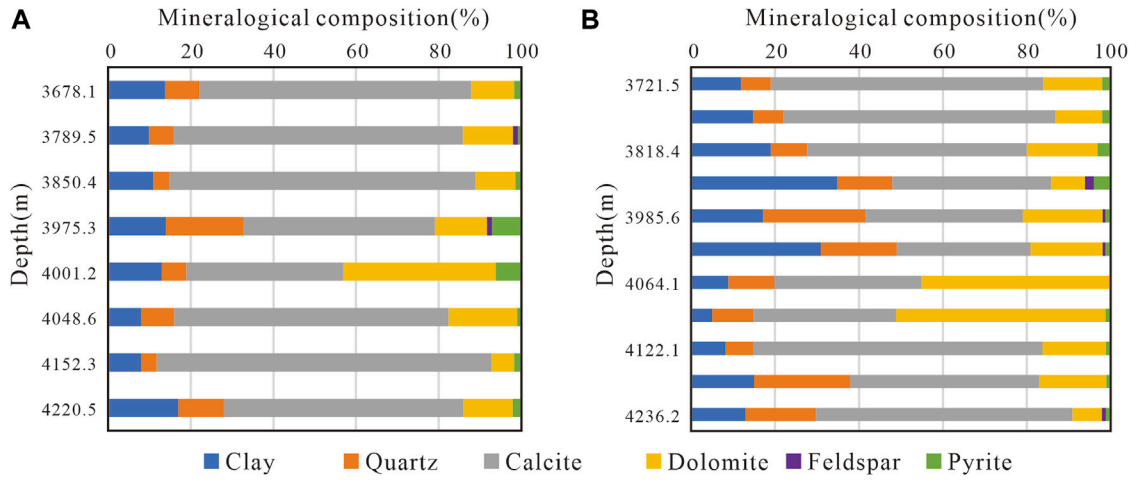

FIGURE 4
Bar chart of mineral components in marl reservoir: **(A)** mineral composition of the laminated marl reservoir; **(B)** mineral composition of the massive marl reservoir.

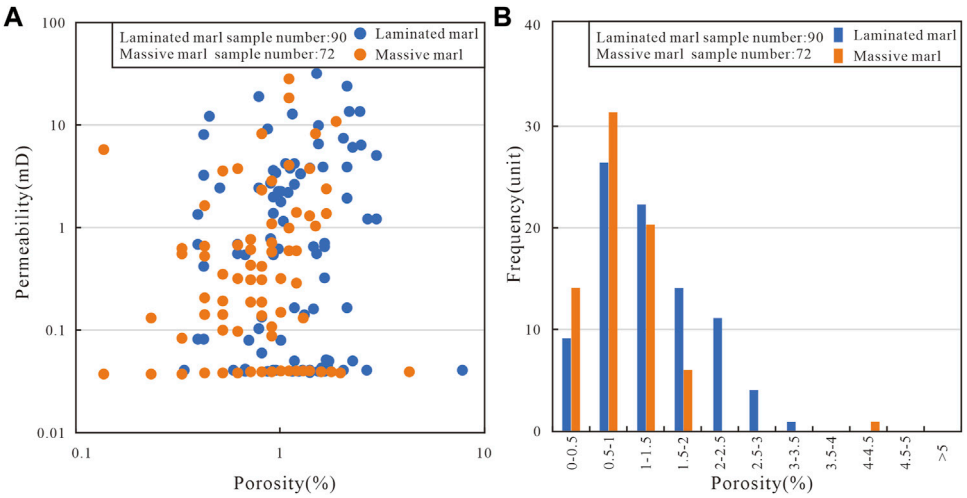

FIGURE 5
Marl reservoir porosity distribution and the porosity-permeability relationship of Shahejie Formation in the Shulu Sag: **(A)**, the relationship between porosity and permeability; **(B)**, reservoir porosity distributions showing the porosity variation mainly in the range of 0–2.5%.

Petrophysical properties

Helium porosity measured in the laboratory represents the connected porosity of rock samples. Laboratory helium porosity tests show that the porosity of laminated marl was slightly higher than that of massive marl (Figure 5A). The porosity of marl ranged from 0.34 to 13.19%, with an average of 1.61% (Figure 5A), mostly varying in the range of 0–2.5% (Figure 5B). The porosity of laminated marl ranged from 0.34 to 13.19%, with an average of 1.61%. The porosity of massive marl ranged from 0.14 to 4.31%, with an average of 0.92% (Figure 5A). Laboratory permeability tests showed that the average permeability of marl was 2.56mD, and the permeability of laminated and massive marl was relatively small. The average permeability of the former was 3.26 mD, and that of the latter was 1.68 mD. A non-functional relationship between porosity and permeability was noted (Figure 5A).

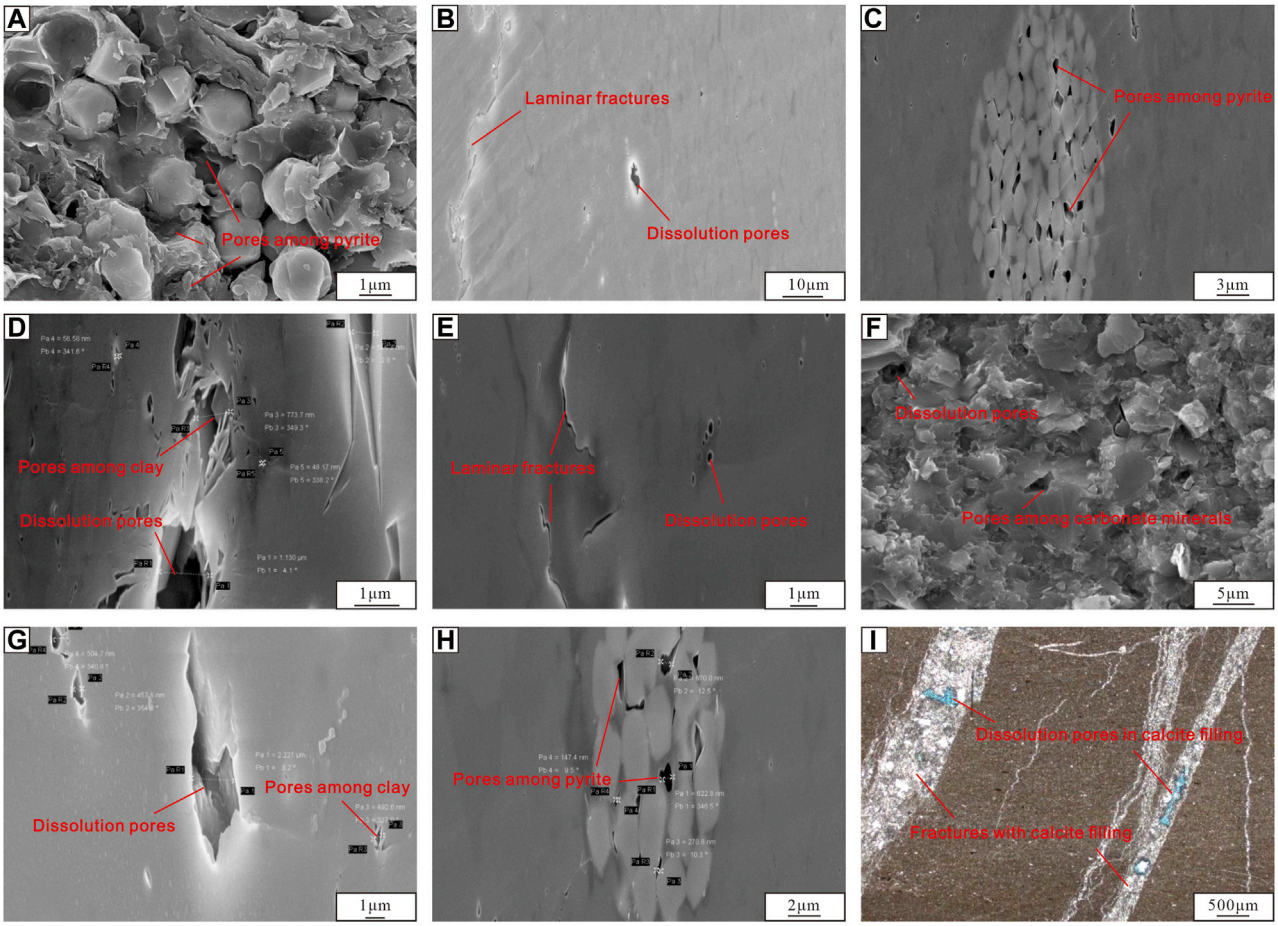

FIGURE 6
Typical pore types found in marl reservoir in the Shulu Sag: **(A)**, intercrystalline pores of pyrite in laminated marl with SEM observation, ST3, 3,670 m; **(B)**, laminar fractures and dissolution pores associated with organic bands in laminated marl, ST3, 3,670.89 m; **(C)**, intercrystalline pores of pyrite in laminated marl, ST3, 3,677.05 m; **(D)**, intercrystalline pores of clay minerals in laminated marl, ST3, 3,978.76 m; **(E)**, nanoscale bedding micro-cracks and dissolution pores in laminated marl, ST3, 3,981.93 m; **(F)**, intercrystalline pores in the massive marl, ST3, 3,999.38 m; **(G)**, dissolution pores and intercrystalline pores of clay minerals in the massive marl, ST3, 3,817.65 m; **(H)**, intercrystalline pores of pyrite in the massive marl, ST3, 3,817.65 m; **(I)**, local dissolution pores occur in calcite, filling in fractures and pore spaces, and they primarily occur concurrently with structural fractures, ST3, 3,983.83 m.

Pore type and pore structure

Based on castings of thin sections and FE-SEM, three types of pores were identified in the marl reservoir. The pores include intercrystalline pores, dissolution pores, and microfractures (Figure 6).

Intercrystalline pores mainly exist between carbonate minerals (Figure 6F), clay minerals (Figures 6D,G), and pyrite (Figures 6C,H). The intercrystalline pore diameter of clay minerals was the largest, and that of carbonate minerals was the smallest. The intercrystalline pore morphology was mainly elongated, curved, and irregular. Intercrystalline pores among pyrite are formed in strawberry pyrite aggregates deposited in a reducing environment. The intercrystalline pore diameters of pyrite in laminated marl were 45–1,185 nm, with a variation range slightly larger than that of massive marl (60–985 nm). The intercrystalline pores among clay minerals were formed during the dehydration transformation process. The intercrystalline pores in marl clay were both nanometer and micron pores. The intercrystalline pores among clay minerals in laminated marl were 90–1815 nm, slightly smaller than those in massive marl (107–2,860 nm). The intercrystalline pore diameters of carbonate minerals in laminated marl were 20–540 nm, slightly larger than those of massive marl (13–125 nm) (Figure 7).

Dissolution pores were widely present in marl reservoirs and were usually densely distributed (Figures 6B,E,G,I). The shape of the dissolution pores was mostly circular, elliptical elongated, or irregular, with the long axis laying along the bedding direction. The Es3 was an important source rock in the Shulu Sag (Huo et al., 2020); thus, the formation of dissolution pores was mainly

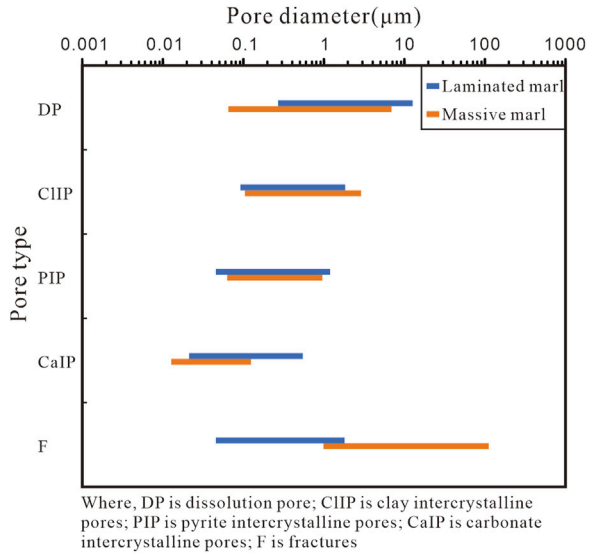

FIGURE 7
Pore diameters distribution range of different types of marl reservoir in the Shulu Sag.

related to organic acid dissolution in the early stage of hydrocarbon generation (Zhou et al., 2020). The dissolution pores appeared to be circular, elliptical elongated, or irregular. The long axis of the dissolution hole was parallel to the bedding direction (Figure 6B). The dissolution pores of the marl reservoir were mainly nanometer pores, with a certain amount of micron pores. The range of dissolution pores of laminated marl was 260 nm–12.2 μm, significantly larger than that of massive marl at 60 nm–7.1 μm (Figure 7).

The microfractures in the marl reservoir can be divided into laminar and structural fractures (Figures 6B,E). Laminar fractures were mainly formed in the laminar marl. Noticeably, due to the difference in mineral composition and sedimentary mode, laminar fractures were easily formed in the diagenetic process of the laminar marl. Laminar slit widths ranged from 45 to 1860 nm, mainly on the nanometer scale, with a small amount of micron-scale. Under the action of regional tectonic stress, marl with a high brittle mineral content easily produced structural fractures (Figure 6I). The filling material of the structural fractures was mainly calcite. Secondary dissolved pores were also found in calcite veins (Figure 6I). The width of structural fractures ranged from 1 to 11 μm, mainly on the micron scale (Figure 7).

Pore-throat size distribution

The MICP test results of the nine marl samples are shown in Figure 8. The mercury injection curve of laminated marl was characterized by a lower displacement pressure, higher mercury saturation, and higher mercury withdrawal rate. The capillary pressure curve showed a double-step characteristic (Figure 8A). The results show that the pore-throat structure of laminated marl was complex, and the micron and nanometer scale pores were well-developed (Figure 8B). The laminated marl was characterized by a double porosity medium of lamination fracture-pore.

Compared with the laminated marl, the mercury injection curve of the massive marl exhibited higher displacement pressure, lower mercury intake saturation, and mercury withdrawal rate for the massive marl. The 'single step' characteristic of the capillary pressure curve was noticeable (Figure 8C). The results revealed that the massive marl reservoir exhibited poor pore connectivity, mainly nanoscale-pores (Figure 8D), which were not conducive to fluid flow.

The marl comprehensive pore distribution can be reflected by the NMR T_2 spectrum (Wu et al., 2021; Zhao et al., 2022). The T_2 spectrum of laminated marl revealed clear bimodal characteristics (Figure 9A), and the right peak was more noticeable, indicating that laminated marl developed not only nanometer micropores but also a certain amount of micrometer macropores. The massive marl showed a single-peak T_2 spectrum (Figure 9B), with the main peak on the left, indicating that nanometer micropores dominated the massive marl, with a few micrometer pores.

In the micro-CT scanning experiment, the greater resolution allowed for a detailed understanding of the size of material components (Wu et al., 2019b, 2020d; Wu et al., 2020e; Wu et al., 2022b). The small pixels were identified as a set of large pixels. Therefore, the connected pores could be identified as macro pore aggregates. A micro-CT scan showed that the laminated marl pores were mainly distributed along the dark lamina with good connectivity (Figure 10A). The massive marl had fewer pores, which were isolated and uniform (Figure 10B).

Discussion

Influence of original sedimentary environment on reservoir quality

The physical properties of the reservoir are mainly affected by the original sedimentary and diagenetic processes (Liu et al., 2016; Zhu et al., 2017; Lu and Liu, 2021), among which, the sedimentary mechanism was the most important. Specifically, the original sedimentary environment and mechanism determine the material basis of the reservoir, while the subsequent geological processes only modify it.

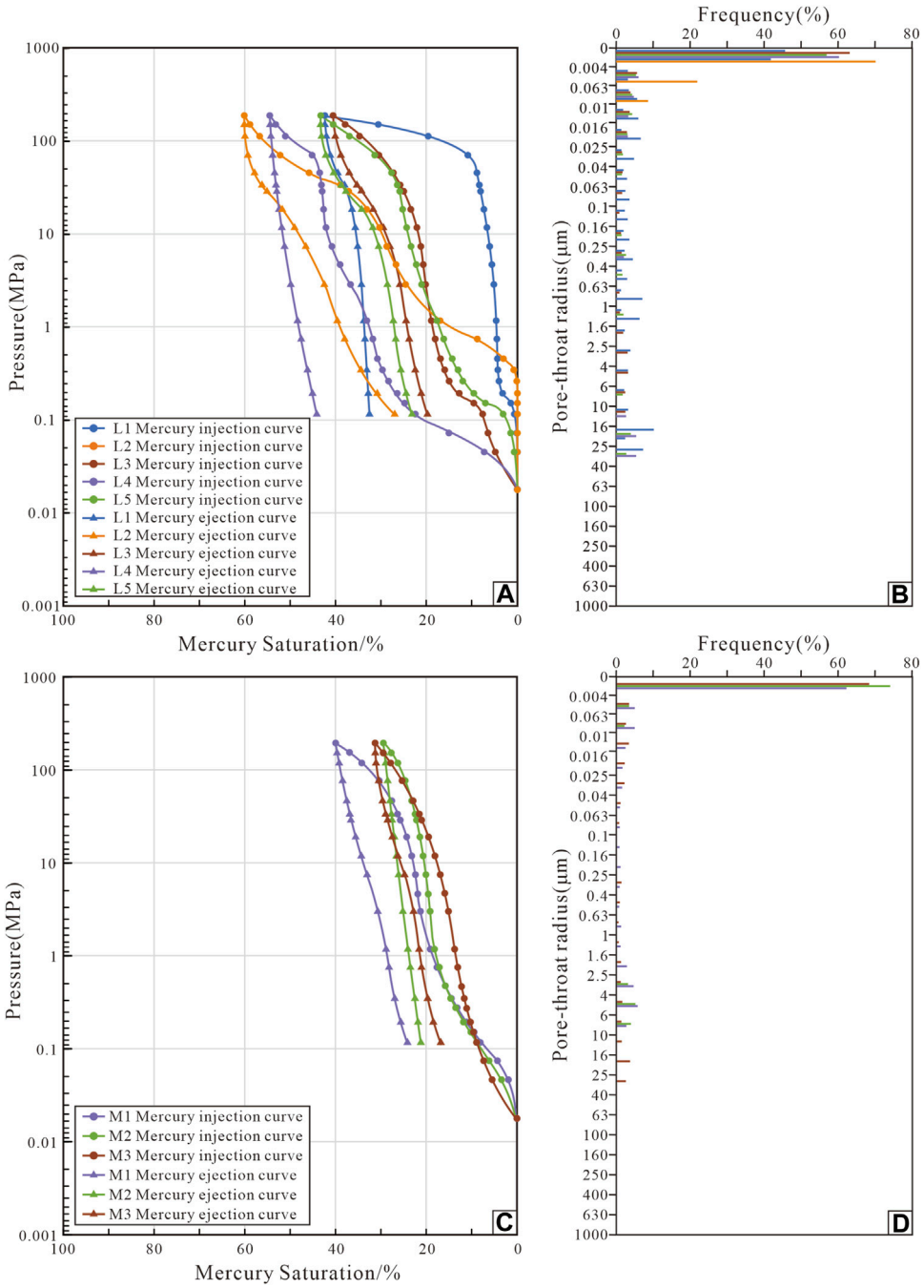

FIGURE 8
Intrusion-extrusion curves and pore size distribution by mercury intrusion capillary pressure (MICP) experiments for tight marl samples in the Shahejie Formation in the Shulu Sag: **(A,B)**, laminated marl reservoir; **(C,D)**, massive marl reservoir.

The sedimentary environment of the lower E_2s_3 strata in the Shulu Sag is characterized by shallow to deep lake subfacies. From the sag slope to the trough area, the water gradually deepened. This sedimentary environment determined the marl of the stratum under E_2s_3, characterized by abundant organic matter enrichment. Drilling confirmed that the thickness of marl in the study area exceeded 1,200 m (Zhao et al., 2014a), providing an ideal environment for the marl to function as a reservoir in the study area.

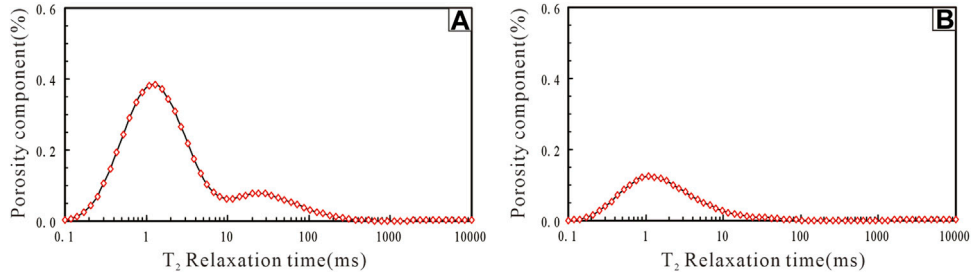

FIGURE 9
The saturated NMR T_2 spectra of marl: **(A)**, laminated marl, ST1, 4257 m; **(B)**, massive marl, ST1, 4263 m.

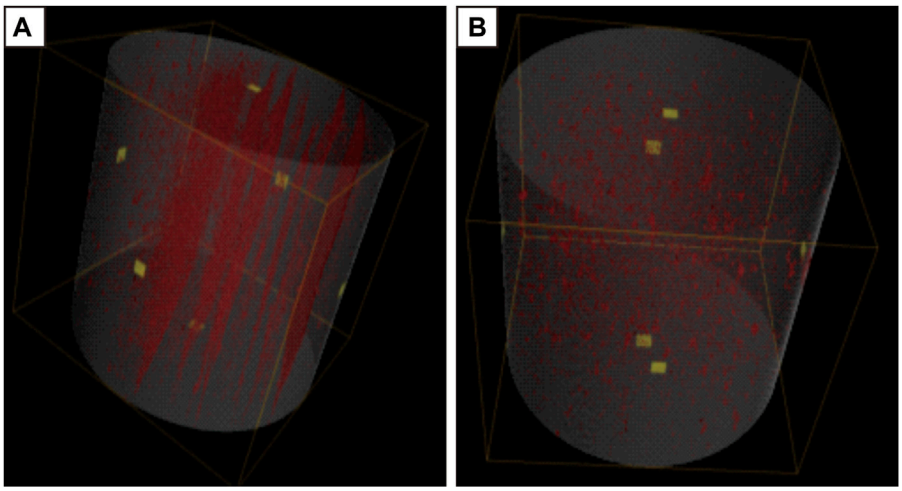

FIGURE 10
Micro-CT showing the 3D pore and connectivity in the marl reservoir: **(A)**, laminated marl, ST3, 3,670.89 m; **(B)**, massive marl, ST3, 3,817.65 m.

The laminated marl in the Shulu Sag is mainly a rhythmic lamination affected by seasonal factors (Fu et al., 2019). The seasonal rhythmic laminae have an apparent binary structure, which consists of chemically deposited carbonate minerals and clastic grains stemming from physical deposition. Laminated marl mainly occurs in shallow and semi-deep lakes near the provenance. The laminated marl had a large pore space, good horizontal connectivity, and its organic matter exhibited continuous distribution in a large area, rendering it an ideal reservoir for oil and gas enrichment (Figure 3L, Figure 3N).

During the formation of the massive marl near the provenance, terrigenous clasts were formed in the sediments. These clasts are rich in organic matter and have the potential for hydrocarbon generation. However, when the massive marl was formed away from the provenance, the carbonate rocks primarily experienced *in situ* chemical deposition.

Influence of rock composition on reservoir quality

Quartz

The presence and content of quartz minerals in marl reportedly affect the pore type and structure (Zhu et al., 2022). The cross plot of quartz content and total porosity reveals a positive correlation between quartz content and total porosity (Figure 11A). The compaction of hard quartz minerals is good for pore preservation, resulting in the development of several intercrystalline pores (Figures 6A,F) in marl reservoirs. Compared with laminated marl, the quartz content in massive marl was expectedly higher, explaining why the massive marl is more likely to produce structural fractures than laminated marl. Influenced by the sedimentary environment of the deep and semi-deep lake, the supply of terry-derived material is limited, and the quartz

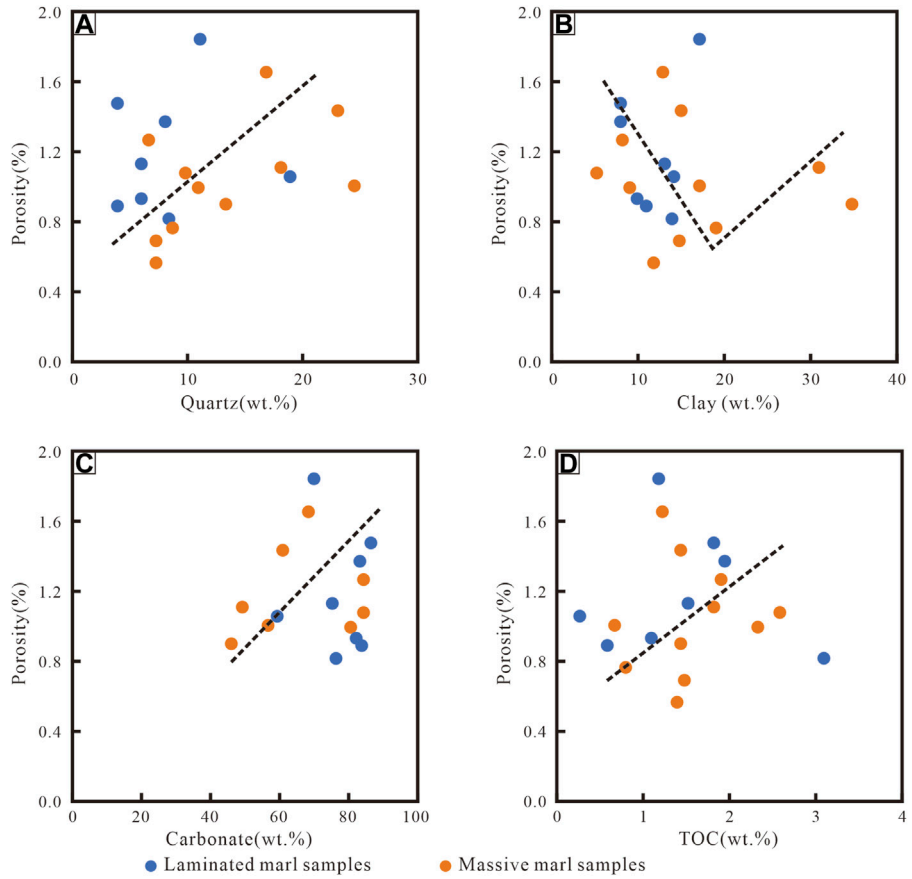

FIGURE 11
Relationships between the material composition and porosity of the marl samples from the ST1, Shulu Sag: **(A)**, relationship between quartz content and total porosity; **(B)**, relationship between clay content and total porosity; **(C)**, relationship between carbonate content and total porosity; **(D)**, relationship between TOC content and total porosity.

content in marl is relatively modest, generally ranging from 5 to 25%.

Clay

With the increase in clay mineral content, the total porosity of marl first decreased first and then increased (Figure 11B). When the content of clay minerals was low, the clay minerals were more plastic and tended to seal intercrystalline pores of carbonate minerals under compaction, resulting in the underdevelopment and poor continuity of nano-pores. Therefore, clay mineral content inversely correlated with the total porosity. As the content of clay minerals increased, they absorbed a great amount of organic matter, which was conducive to the development of dissolution pores in hydrocarbon generation and acid discharge. In addition, intercrystalline pores of clay minerals were formed in large quantities and had good connectivity. Therefore, when the clay mineral content exceeded a certain amount, it positively correlated with the total porosity. This threshold was approximately 15% in laminated marl 20% in massive marl. Nevertheless, it is essential to note that marl porosity does not increase indefinitely as the mud content continues to increase beyond this threshold due to the influence of marl rock skeleton and organic acid production.

Carbonate minerals

The marl is rich in carbonate minerals; its content generally ranges of 50–90%. Carbonate minerals are an important determinant of total porosity; and these two elements show a positive correlation in the cross plot (Figure 11C). The existence of carbonate minerals is conducive to the subsequent formation of dissolution pores (Figures 6B,E,G). In addition, the brittle carbonate minerals tended to produce fractures under the action of tectonic stress, increasing pore connectivity (Figure 6I).

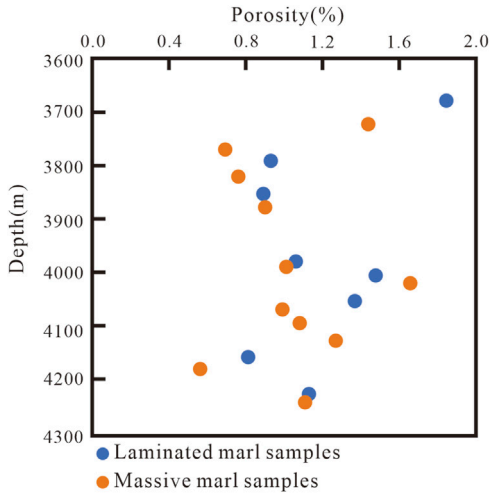

FIGURE 12
Relationship between depth and total porosity of the marl samples from the ST1, Shulu Sag.

TOC

The marl in the study area is an important source of rock that is rich in organic matter and exhibits self-generation and self-storage (Huo et al., 2020). Previous studies showed that TOC content in marl increased significantly from shallow lake subfacies to deep lake subfacies (Zhao et al., 2015). In this study, TOC content was mainly distributed in the range of 1–4%. In the process of hydrocarbon generation, the organic acids associated with marl rich in organic matter catalyze dissolution, directly leading to the formation of dissolution pores. Therefore, TOC content in marl was positively correlated with total porosity (Figure 11D).

Influence of diagenesis and tectonism on reservoir quality

Diagenesis shapes the porosity and permeability of sedimentary basins (Rahman and Worden, 2016; Wang et al., 2021; Du et al., 2022). During the diagenetic process of marl, compaction, cementation, and dissolution are the key geological processes driving the formation and development of marl reservoir space. Moreover, regional and local post-diagenetic tectonism is critical for reservoir transformation.

Compaction

Under compaction, burial depth and the porosity of the clastic reservoir are inversely correlated (Zhu et al., 2019a; Zhang et al., 2020). However, the porosity of the marl reservoir did not decrease with increasing depth (Figure 12), mainly because marl is different from a clastic rock; in the early diagenetic stage, many primary intercrystalline pores are cemented and filled, and in the subsequent deep burial stage, burial depth compaction has little influence on reservoir porosity. Simultaneously, as a large amount of organic matter in marl gradually reaches maturity, it generates hydrocarbon and organic acids. Finally, large dissolution pores are formed, translating to an increased porosity in the marl.

Dissolution

Dissolution significantly improves the quality of the marl reservoir (Yang et al., 2022). SEM revealed the widespread dissolution pores with large diameters (Figures 6B,E,G,I). Dissolution mainly occurs in the margins and interiors of calcite, dolomite, and clay minerals. Dissolution pores are generally elliptic or elongated, irregularly shaped with the long axis parallel to the bedding direction. As mentioned above, dissolution pores in laminated marl were mainly nanoscale pores with a certain amount of micron-scale pores developed along the bedding direction. In this case, the mercury injection curve showed double-step features (Figure 8A), and the T_2 spectrum revealed a double peak (Figure 9A). Dissolution pores are formed in marl under the action of acids, leading to a spatial fracture network characterized by smooth fluid flow and improved reservoir quality.

Tectonism

Marl is rich in brittle carbonate minerals. The content of brittle minerals was higher in massive marl, than in laminated marl. Marl, especially massive marl, is prone to produce structural fractures under regional tectonic stress. The diameter of structural fractures was usually 1-2 orders of magnitude larger than the pore diameter (Figure 7). Of note, the structure fracture had higher porosity than the pores (Figure 6I), significantly improving the physical properties of the marl reservoir (Kong et al., 2019). After the marl diagenesis, Shulu Sag underwent many tectonic movements, and many faults were formed (Zhao et al., 2015; Zhu et al., 2018; Zhu et al., 2019b; Zhu et al., 2020; He et al., 2022). The vicinity of these faults tended to be characterized by a concentration of stress, which was conducive to the occurrence of microfractures associated with faults, which played a key role in improving the physical features of the reservoir. The analysis of the physical properties of marl showed that the permeability of massive marl exceeded 10mD due to structural fractures. However, the permeability was mainly in the range of 0.1-1mD in the absence of structural fractures (Figure 5A). In laminated marl, most fractures were laminated fractures (Figures

3A,C,E), which can also improve the permeability of laminated marl (Figure 5A).

Conclusion

1) The mineral content of laminated and massive marl differed. The calcite content of laminated marl was higher than that of massive marl, while the content of dolomite, clay minerals, and quartz was lower in laminated marl than in massive marl. The two marl fabrics contained little or no feldspar.
2) Three types of pores were developed in the marl reservoir of Shulu Sag, namely, intercrystalline pores, dissolution pores, and microfractures. The intercrystalline and dissolution pores of laminated marl were slightly larger than those of massive marl. Lamellar fractures were formed mainly in laminated marl, whereas microfractures were primarily associated with massive marl and were prone to calcite filling.
3) Laminated marl presented better physical property than massive marl. The micron and nanometer pores of laminated marl were well-developed with lamellar fissures and pores, as well as good connectivity. However, the massive marl reservoir had poor pore connectivity and was dominated by nanoscale pores, not conducive to fluid flow. The massive marl presented a few isolated and uniform holes.
4) The physical properties of the marl reservoir in Shulu Sag were mainly driven by sedimentation and diagenesis. Seasonal factors and the relationship with the provenance location were the main drivers of physical differentiation between laminated and massive marl reservoirs. In addition, the high quartz content and TOC were conducive to the formation of 'sweet spot' reservoirs. Compaction depth was beneficial to hydrocarbon generation and the acid discharge of organic matter to improve reservoir quality. Dissolution and tectonism shaped the construction of reservoirs.

Data availability statement

The original contributions presented in the study are included in the article/Supplementary Material, further inquiries can be directed to the corresponding author.

Author contributions

JL: investigation, methodology, writing—original draft, and data analysis. GF: supervision and writing—review and editing. DZ: writing—review and editing. LC: writing—original draft and processing the data. ZlL: writing—review and editing. YL: supervision and writing—review and editing. WL: methodology—original draft. MH: methodology—review and editing. ZeL: writing—review and editing.

Funding

This work was supported by the National Natural Science Foundation of China (41602154), CNPC Innovation Foundation (2015D-5006-0103), and Projects of Talents Recruitment of GDUPT (2018rc01).

Acknowledgments

Special thanks go to Zhanwen Yu from PetroChina Huabei Company. His constructive suggestions and manuscript review positively influenced this research and article writing.

Conflict of interest

DZ was employed by the Company BGP Inc.

LC was employed by the PetroChina Huabei Company.

ZL was employed by the Data Acquisition Branch and Geo-Logging Company.

The remaining authors declare that the research was conducted in the absence of any commercial or financial relationships that could be construed as a potential conflict of interest.

The reviewer CM declared a shared affiliation with the authors GF and YL to the handling editor at the time of review.

Publisher's note

Supplementary material

The Supplementary Material for this article can be found online at: https://www.frontiersin.org/articles/10.3389/feart.2022.1016122/full#supplementary-material

References

Bordignon, F., Figueiredo, L. D., Exterkoetter, R., Rodrigues, B., and Duarte, M. (2019). "Deep learning for grain size and porosity distributions estimation on micro-CT images," in *Proceedings of the 16th international congress of the Brazilian geophysical Societye&Expogef (Radiology)* (Rio de Janeiro: SBGf - Sociedade Brasileira de Geofísica). doi:10.22564/16cisbgf2019.209

Cui, J., Yuan, X., Wu, S., Zhang, R., Jin, S., and Li, Y. (2021). Rock types and reservoir characteristics of shahejie formation marl in shulu sag, jizhong depression, bohai bay basin. *J. Earth Sci.* 32 (4), 986–997. doi:10.1007/s12583-020-1092-5

Cui, Z., Guo, Y., Li, Y., Wu, J., Li, B., Li, C., et al. (2015). Calcilutite-rudstone petrological characteristics in the lower part of Member 3 of Shahejie formation, Shulu sag. *Acta Pet. Sin.* 36 (S1), 21–30. doi:10.7623/syxb2015S1003

Du, X., Tian, C., Wang, Y., Liu, Z., and Qin, G. (2022). Sedimentary and reservoir characteristics of an Oligocene-Miocene mixed siliciclastic-carbonate succession in southeast Iraq. *Mar. Pet. Geol.* 138, 105533. doi:10.1016/j.marpetgeo.2022.105533

Fu, X., Wu, J., Shou, J., Wang, X., Zhou, J., Zhang, T., et al. (2019). Tight oil reservoir characteristics of lacustrine mixed marlstone in the palaeogene Shahejie Formation of shulu sag, bohai Bay Basin. *Oil GAS J.* 40 (01), 78–91. doi:10.11743/ogg20190108

Guo, W., Dong, C., Lin, C., Wu, Y., Zhang, X., and Liu, J. (2022). Rock physical modeling of tight sandstones based on digital rocks and reservoir porosity prediction from seismic data. *Front. Earth Sci. (Lausanne).* 10, 932929. doi:10.3389/feart.2022.932929

Han, C., Tian, J., Zhao, R., Luo, D., Qu, Y., Yu, Z., et al. (2015). Reservoir space types and its Genesis in tight calcilutite-rudstone reservoir of the lower part of Member 3 of Shahejie Formation, Shulu sag. *Acta Pet. Sin.* 36 (S1), 31–39. doi:10.7623/syxb2015S1004

He, J., Wang, J., Yu, Q., Cheng, C., and Milsch, H. (2022). Stress-Dependent permeability of naturally Micro-Fractured shale. *Geosciences* 12 (4), 150. doi:10.3390/geosciences12040150

He, J., Wang, J., Yu, Q., Liu, W., Ge, X., Yang, P., et al. (2018). Pore structure of shale and its effects on gas storage and transmission capacity in well HD-1 eastern Sichuan Basin, China. *Fuel* 226, 709–720. doi:10.1016/j.fuel.2018.04.072

Hou, H., Shao, L., Li, Y., Li, Z., Zhang, W., and Wen, H. (2018). The pore structure and fractal characteristics of shales with low thermal maturity from the Yuqia Coalfield, northern Qaidam Basin, northwestern China. *Front. Earth Sci.* 12 (1), 148–159. doi:10.1007/s11707-016-0617-y

Huo, Z., Tang, X., Meng, Q., Zhang, J., Li, C., Yu, X., et al. (2020). Geochemical characteristics and hydrocarbon expulsion of lacustrine marlstones in the shulu sag, bohai bay basin, eastern China: Assessment of tight oil resources. *Nat. Resour. Res.* 29 (4), 2647–2669. doi:10.1007/s11053-019-09580-8

James, W., Schmoker, T, C., and Hester, C. (1983). Organic carbon in bakken formation, United States portion of williston basin. *Am. Assoc. Pet. Geol. Bull.* 67, 2165–2174. doi:10.1306/ad460931-16f7-11d7-8645000102c1865d

Jia, C., Zheng, M., and Zhang, Y. (2012a). Unconventional hydrocarbon reserces in China and the prospect of exploration and development. *Petroleum Explor. Dev.* 39 (02), 129–136.

Jia, C., Zou, C., Li, J., Li, D., and Zheng, M. (2012b). Assessment criteria, main types, basic features and resource prospects of the tight oil in China. *Acta Pet. Sin.* 33 (03), 343–350.

Jiang, S., and Mokhtari, M. (2019). Characterization of marl and interbedded limestone layers in the Eagle Ford Formation, DeWitt county, Texas. *J. Pet. Sci. Eng.* 172, 502–510. doi:10.1016/j.petrol.2018.09.094

Jiang, Z., Chen, D., Qiu, L., Liang, H., and Ma, J. (2007). Source-controlled carbonates in a small eocene half-graben lake basin (shulu sag) in central hebei province, north China. *Sedimentology* 54 (2), 265–292. doi:10.1111/j.1365-3091.2006.00834.x

Kong, X., Jiang, Z., Han, C., and Zhang, R. (2020). Organic matter enrichment and hydrocarbon accumulation models of the marlstone in the shulu sag, bohai Bay Basin, northern China. *Int. J. Coal Geol.* 217, 103350. doi:10.1016/j.coal.2019.103350

Kong, X., Jiang, Z., Han, C., Zheng, L., Yang, Y., and Liu, Y. (2016). Laminations characteristics and reservoir significance of fine-grained carbonate in the lower 3rd member of Shahejie Formation of Shulu sag. *Petroleum Geol. Recovery Effic.* 23 (4), 19–26. doi:10.3969/j.issn.1009-9603.2016.04.003

Kong, X., Jiang, Z., Han, C., Zheng, L., and Zhang, J. (2019). The tight oil of lacustrine carbonate-rich rocks in the Eocene Shulu Sag: Implications for lithofacies and reservoir characteristics. *J. Pet. Sci. Eng.* 175, 547–559. doi:10.1016/j.petrol.2018.12.028

Li, J., Fu, G., and Liu, Z. (2022). Quantitative characterization of the lower limit of the physical properties of tight oil reservoirs in Nano-Material porous media. *Integr. Ferroelectr.* 227 (1), 288–303. doi:10.1080/10584587.2022.2072118

Li, Q., Jiang, Z., You, X., Zhao, X., and Zhang, R. (2016). Role of organic facies in evaluation of unconventional petroleum reservoirs: A case study of organic-matterrich marlstone reservoirs in the shulu sag. *J. Northeast Petroleum Univ.* 40 (03), 1–9. doi:10.3969/j.issn.2095-4107.2016.03.001

Liang, H., Kuang, H., Liu, J., Guo, Y., and Su, J. (2007). Discussion on origin for marls of the member 3 of Shahejie Formation of Paleogene in Shulu sag of central Hebei depression. *J. Palaeogeogr.* 02, 167–174. doi:10.3969/j.issn.1671-1505.2007.02.005

Lin, S., Zou, C., Yuan, X., and Yang, Z. (2011). Status quo of tight oil exploitation in the United States and its implication. *Lithol. Reserv.* 23 (04), 25–30. doi:10.3969/j.issn.1673-8926.2011.04.005

Liu, E., Liu, C., Shi, D., Zhu, D., Xu, Q., and Wang, Y. (2022). Characterization and control of pore structural heterogeneity for low-thermal-maturity shale: A case study of the shanxi Formation in the northeast zhoukou depression, southern north China basin. *Front. Earth Sci. (Lausanne).* 10, 943935. doi:10.3389/feart.2022.943935

Liu, M., and Grana, D. (2018). Stochastic nonlinear inversion of seismic data for the estimation of petroelastic properties using the ensemble smoother and data reparameterization. *Geophys. J. Soc. Explor. Geophys.* 83 (3), M25–M39. doi:10.1190/GEO2017-0713.1

Liu, X., Rendle-Bühring, R., Meyer, I., and Henrich, R. (2016). Holocene shelf sedimentation patterns off equatorial East Africa constrained by climatic and sea-level changes. *Sediment. Geol.* 331, 1–11. doi:10.1016/j.sedgeo.2015.10.009

Liu, Z., Li, W., Li, J., Wang, W., Fu, G., and Zhang, H. (2022a). Characteristics of tight oil reservoir based on nano-CT. *Adv. Mater. Sci. Eng.* 2022, 1–11. doi:10.1155/2022/7863047

Liu, Z., Li, W., Zhang, L., and Li, J. (2022b). Petrophysical properties of tight marl reservoir and its influence on fluid percolation capacity. *Integr. Ferroelectr.* 227 (1), 273–287. doi:10.1080/10584587.2022.2072116

Liu, Z., Yu, Z., Lv, Y., and Li, J. (2020). Characteristics and oil content of tight oil marl reservoirs in Es3L of shulu sag. *J. Guangdong Univ. Petrochem. Technol.* 30 (04), 1–4. doi:10.3969/j.issn.2095-2562.2020.04.001

Lu, Y., and Liu, K. (2021). Pore structure characterization of eocene Low-Permeability sandstones via fractal analysis and machine learning: An example from the dongying depression, bohai bay basin, China. *ACS Omega* 6 (17), 11693–11710. doi:10.1021/acsomega.1c01015

Miller, B. A., Paneitz, J. M., Mullen, M. J., Meijs, R., Tunstall, K. M., and Garcia, M. (2008). "The successful application of a compartmental completion technique used to isolate multiple Hydraulic-Fracture treatments in horizontal bakken shale wells in North Dakota," in SPE Annual Technical Conference and Exhibition, September 21–24, 2008 (Denver, Colorado, USA: Society of Petroleum Engineers), 1–11. doi:10.2118/116469-MS

Qian, Y., Gao, P., Fang, X., Sun, F., Cai, Y., and Zhou, Y. (2022). Microstructure characterization techniques for shale reservoirs: A review. *Front. Earth Sci. (Lausanne).* 10, 930474. doi:10.3389/feart.2022.930474

Qiu, L., Jiang, Z., Liang, H., Li, C., and Sun, B. (2010). Limemudstone: A kind of carbonate rock of terrigenous mechanical origin. *J. China Univ. Petroleum* 34 (06), 1–7. doi:10.3969/j.issn.1673-5005.2010.06.001

Rahman, M. J. J., and Worden, R. H. (2016). Diagenesis and its impact on the reservoir quality of miocene sandstones (surma group) from the bengal basin, Bangladesh. *Mar. Pet. Geol.* 77, 898–915. doi:10.1016/j.marpetgeo.2016.07.027

Shan, C. A., Zhang, T., Wei, Y., and Zhang, Z. (2017). Shale gas reservoir characteristics of Ordovician-Silurian formations in the central Yangtze area, China. *Front. Earth Sci.* 11 (1), 184–201. doi:10.1007/s11707-016-0565-4

Wang, D., Ning, F., Lu, J., Lu, H., Kang, D., Xie, Y., et al. (2021). Reservoir characteristics and critical influencing factors on gas hydrate accumulations in the Shenhu area, South China Sea. *Mar. Pet. Geol.* 133, 105238. doi:10.1016/j.marpetgeo.2021.105238

Wu, J., Yang, S., Gan, B., Cao, Y., Zhou, W., Kou, G., et al. (2021). Pore structure and movable fluid characteristics of typical sedimentary lithofacies in a tight conglomerate reservoir, mahu depression, northwest China. *ACS Omega* 6 (36), 23243–23261. doi:10.1021/acsomega.1c02952

Wu, Y., Lin, C., Ren, L., Yan, W., An, S., Chen, B., et al. (2018). Reconstruction of 3D porous media using multiple-point statistics based on a 3D training image. *J. Nat. Gas. Sci. Eng.* 51, 129–140. doi:10.1016/j.jngse.2017.12.032

Wu, Y., Lin, C., Yan, W., Liu, Q., Zhao, P., and Ren, L. (2020a). Pore-scale simulations of electrical and elastic properties of shale samples based on multicomponent and multiscale digital rocks. *Mar. Pet. Geol.* 117, 104369. doi:10.1016/j.marpetgeo.2020.104369

Wu, Y., Tahmasebi, P., Lin, C., and Dong, C. (2020c). A comprehensive investigation of the effects of organic-matter pores on shale properties: A multicomponent and multiscale modeling. *J. Nat. Gas. Sci. Eng.* 81, 103425. doi:10.1016/j.jngse.2020.103425

Wu, Y., Tahmasebi, P., Lin, C., and Dong, C. (2020b). Process-based and dynamic 2D modeling of shale samples: Considering the geology and pore-system evolution. *Int. J. Coal Geol.* 218, 103368. doi:10.1016/J.COAL.2019.103368

Wu, Y., Tahmasebi, P., Lin, C., and Dong, C. (2022a). Using digital rock physics to investigate the impacts of diagenesis events and pathways on rock properties. *J. Pet. Sci. Eng.* 208, 108025. doi:10.1016/j.petrol.2020.108025

Wu, Y., Tahmasebi, P., Lin, C., Ren, L., and Dong, C. (2019a). Multiscale modeling of shale samples based on low- and high-resolution images. *Mar. Pet. Geol.* 109, 9–21. doi:10.1016/j.marpetgeo.2019.06.006

Wu, Y., Tahmasebi, P., Lin, C., Ren, L., and Zhang, Y. (2020d). Quantitative characterization of non-wetting phase in water-wet porous media based on multiphase flow experiment and numerical simulation(Article). *J. Pet. Sci. Eng.* 188, 106914. doi:10.1016/j.petrol.2020.106914

Wu, Y., Tahmasebi, P., Lin, C., Zahid, M. A., Dong, C., Golab, A. N., et al. (2019b). A comprehensive study on geometric, topological and fractal characterizations of pore systems in low-permeability reservoirs based on SEM, MICP, NMR, and X-ray CT experiments. *Mar. Pet. Geol.* 103, 12–28. doi:10.1016/j.marpetgeo.2019.02.003

Wu, Y., Tahmasebi, P., Liu, K., Fagbemi, S., Lin, C., An, S., et al. (2022b). Two-phase flow in heterogeneous porous media: A multiscale digital model approach. *Int. J. Heat. Mass Transf.* 194, 123080. doi:10.1016/j.ijheatmasstransfer.2022.123080

Wu, Y., Tahmasebi, P., Yu, H., Lin, C., Wu, H., and Dong, C. (2020e). Pore-scale 3D dynamic modeling and characterization of shale samples: Considering the effects of thermal maturation. *J. Geophys. Res. Solid Earth* 125 (1), e2019J–e18309J. doi:10.1029/2019JB018309

Yang, J., Zhang, J., Ji, Y., Lv, W., Wu, H., He, Z., et al. (2022). Pore structure characteristics and controlling factors of a tight sandstone reservoir in the paleogene shahejie formation, nanpu sag, bohai bay basin, China. *ACS Omega* 7 (2), 1740–1756. doi:10.1021/acsomega.1c04573

Zhang, J., Liu, G., Torsaeter, O., Tao, S., Jiang, M., Li, G., et al. (2020). Pore-throat structure characteristics and its effect on flow behavior in Gaotaizi tight siltstone reservoir, northern Songliao Basin. *Mar. Pet. Geol.* 122, 104651. doi:10.1016/j.marpetgeo.2020.104651

Zhang, R., Chen, K., Zhu, J., Tang, X., Yu, Z., Zhang, Y., et al. (2021). Tight gas reservoir forming condition and resource potential in the lacustrine carbonate in the middle-deep layer of Shulu Sag of Jizhong Depression,Bohai Bay Basin. *Nat. Gas. Geosci.* 32 (05), 623–632. doi:10.11764/j.issn.1672-1926.2020.12.004

Zhang, S., Tang, S., Zhang, J., and Pan, Z. (2018). Pore structure characteristics of China sapropelic coal and their development influence factors. *J. Nat. Gas. Sci. Eng.* 53, 370–384. doi:10.1016/j.jngse.2018.03.022

Zhao, F., Dong, Z., Wang, C., Zhang, W., and Yu, R. (2022). Pore connectivity characteristics and controlling factors for black shales in the Wufeng-Longmaxi formation, southeastern sichuan basin, China. *Energies* 15 (8), 2909. doi:10.3390/en15082909

Zhao, L., Qin, X., Han, D., Geng, J., Yang, Z., and Cao, H. (2016). Rock-physics modeling for the elastic properties of organic shale at different maturity stages. *Geophys. J. Soc. Explor. Geophys.* 81 (5), D527–D541. doi:10.1190/GEO2015-0713.1

Zhao, X., Jiang, Z., Zhang, R., Li, H., Yang, D., Cui, Z., et al. (2015). Geological characteristics and exploration practices of special-lithology tight oilreservois in continental rift basinsi a case sludy of tight oil in Sha-hejie Formation, Shulu sag. *Acta Pet. Sin.* 36 (S1), 1–9. doi:10.7623/syxb2015S1001

Zhao, X., Li, Q., Jiang, Z., Zhang, R., and Li, H. (2014a). Organic geochemistry and reservoir characterization of the organic matter-rich calcilutite in the shulu sag, bohai Bay Basin, north China. *Mar. Pet. Geol.* 51 (2), 239–255. doi:10.1016/j.marpetgeo.2013.12.014

Zhao, X., Zhu, J., Zhang, R., Yu, Z., Wang, J., and Guo, Y. (2014b). Characteristics and exploration potential of tight calcilutite-rudstone reser-voirs in Shulu sag, Jizhong depression, North China. *Acta Pet. Sin.* 35 (04), 613–622. doi:10.7623/syxb201404001

Zhou, L., Lu, S., Wu, J., and Guo, Y. (2020). Characteristics of tight-oil reservoir and accumulation areaprediction in Lower part of the 3rd Shahejie Formation of Shulu sag. *Geol. Rev.* 66 (S1), 123–125. doi:10.16509/j.georeview.2020.s1.048

Zhu, H., Ju, Y., Huang, C., Chen, F., Chen, B., and Yu, K. (2020). Microcosmic gas adsorption mechanism on clay-organic nanocomposites in a marine shale117256. *Energy* 197, 117256. doi:10.1016/j.energy.2020.117256

Zhu, H., Ju, Y., Huang, C., Han, K., Qi, Y., Shi, M., et al. (2019a). Pore structure variations across structural deformation of silurian longmaxi shale: An example from the chuandong thrust-fold belt. *Fuel* 241, 914–932. doi:10.1016/j.fuel.2018.12.108

Zhu, H., Ju, Y., Qi, Y., Huang, C., and Zhang, L. (2018). Impact of tectonism on pore type and pore structure evolution in organic-rich shale: Implications for gas storage and migration pathways in naturally deformed rocks. *Fuel* 228, 272–289. doi:10.1016/j.fuel.2018.04.137

Zhu, H., Ju, Y., Yang, M., Huang, C., Feng, H., Qiao, P., et al. (2022). Grain-scale petrographic evidence for distinguishing detrital and authigenic quartz in shale: How much of a role do they play for reservoir property and mechanical characteristic? *Energy* 239, 122176. doi:10.1016/j.energy.2021.122176

Zhu, H., Zhang, T., Zhong, D., Li, Y., Zhang, J., and Chen, X. (2019b). Binary pore structure characteristics of tight sandstone reservoirs. *Petroleum Explor. Dev.* 46 (6), 1297–1306. doi:10.1016/S1876-3804(19)60283-1

Zhu, X., Zeng, H., Li, S., Dong, Y., Zhu, S., Zhao, D., et al. (2017). Sedimentary characteristics and seismic geomorphologic responses of a shallow-water delta in the Qingshankou Formation from the Songliao Basin, China. *Mar. Pet. Geol.* 79, 131–148. doi:10.1016/j.marpetgeo.2016.09.018

Zou, C., Zhu, R., Wu, S., Yang, Z., Tao, S., Yuan, X., et al. (2012). Types, characteristics, Genesis and prospeets of eonventional and unconventional hydrocarbon accumulations:Taking tight oil and tight gas in China as an instance. *Aeta Perolei Sin.* 33 (02), 173–187.